

Experimental Investigation of the Impact of Cathode Grade on Sludge Formation at the Cathode Block-Aluminum Interface of Hall–Héroult Cells



JEAN-RENÉ LANDRY, MOJTABA FALLAH FINI, GERVAIS SOUCY,
MARTIN DÉSILETS, PATRICK PELLETIER, LOIG RIVOALAND,
and DIDIER LOMBARD

The presence of resistive sludge on the cathode surface in Hall–Héroult cells can increase the aluminum production costs and reduces cell lifetime. Modern cells with graphitized cathode blocks generally operate satisfactorily but some are exhibiting excessive deposit formation, thus lower performances. Little attention has ever been given to the role of the cathode grade and its properties on sludge formation. In this investigation, five graphitized industrial cathode grades with varying properties are tested on a bench scale aluminum electrolysis setup with cathodic current density of 0.9 A/cm^2 , under a nitrogen atmosphere at 1233 K ($960 \text{ }^\circ\text{C}$) for 8 hours with initial bath composition of 10 pct alumina, cryolite ratio of 2.2, 5 pct CaF_2 and no point feeding. Postmortem characterization includes Rietveld refinement of deposits, optical microscopy and SEM-EDS observations of the carbon-aluminum interface. Sludge located near the center of the cathode surface was generated during the experiments despite the absence of point feeding. The sludge profile was variable among grades and could be related to the horizontal and vertical thermal conductivities of the blocks. This study has pushed further the understanding of the mechanisms of sludge formation and dissolution concerning the cathode grade properties.

<https://doi.org/10.1007/s11663-018-1435-0>

© The Minerals, Metals & Materials Society and ASM International 2018

I. INTRODUCTION

A. The Problem Concerning Sludge

THE main drawback of the Hall–Héroult process is its high electrical energy consumption. The formation and accumulation of electrically resistive sludge (aka *muck*) at the cathode block surface increase the electrical resistance of the cell, which boosts cathode voltage drop (CVD). The net effect is the higher energy requirement and thereby, higher aluminum production costs. Due to high electrical resistance of the sludge compared to the metal, the presence of sludge at the carbon-aluminum interface redirects the electrical current and creates high

current density spots, prompting cathode block electrochemical wear.^[1] Another consequence of the presence of sludge on the cathode surface is the generation of horizontal currents, which increase metal pad movement.^[2] The increased metal flow and resulting oscillation of the bath-metal interface greatly contribute to difficulty in reducing the ACD and increases aluminum solubility, prompting current efficiency losses.^[3,4] The control over the formation of sludge in Hall–Héroult cells is a key factor in avoiding high CVD, current efficiency losses and excessive cathode wear.

B. Description of Deposits

During the regular operation of a typical alumina reduction cell, there is a variety of inevitable deposits that form within the process through time. Figure 1 displays the deposits that occur in modern point feeding cells.

The protective side ledge is necessary in order to avoid molten metal and electrolyte attacks and infiltrations in the sidewall that cause premature cell failures.^[5] Ideally, this frozen layer of bath should cover the entire surface of the side lining. The ledge toe is a horizontal elongation of the side ledge formed on the cathode

JEAN-RENÉ LANDRY, MOJTABA FALLAH FINI, GERVAIS SOUCY, and MARTIN DÉSILETS are with the Université de Sherbrooke, 2500 boul. de l'Université, Sherbrooke, QC J1K 2R1, Canada. Contact e-mail: Gervais.Soucy@USherbrooke.ca PATRICK PELLETIER is with the Rio Tinto, 1955 boul. Mellon, Jonquière, QC G7S 1C5, Canada. LOIG RIVOALAND is with the Carbone Savoie, Notre-Dame-de-Briançon, 73260 Aigueblanche Cedex, France. DIDIER LOMBARD is with the Rio Tinto, LRF, rue Henri Sainte Claire Deville CS 40114, 73 302 Saint Jean de Maurienne, France.

Manuscript submitted July 18, 2018.

Article published online October 25, 2018.

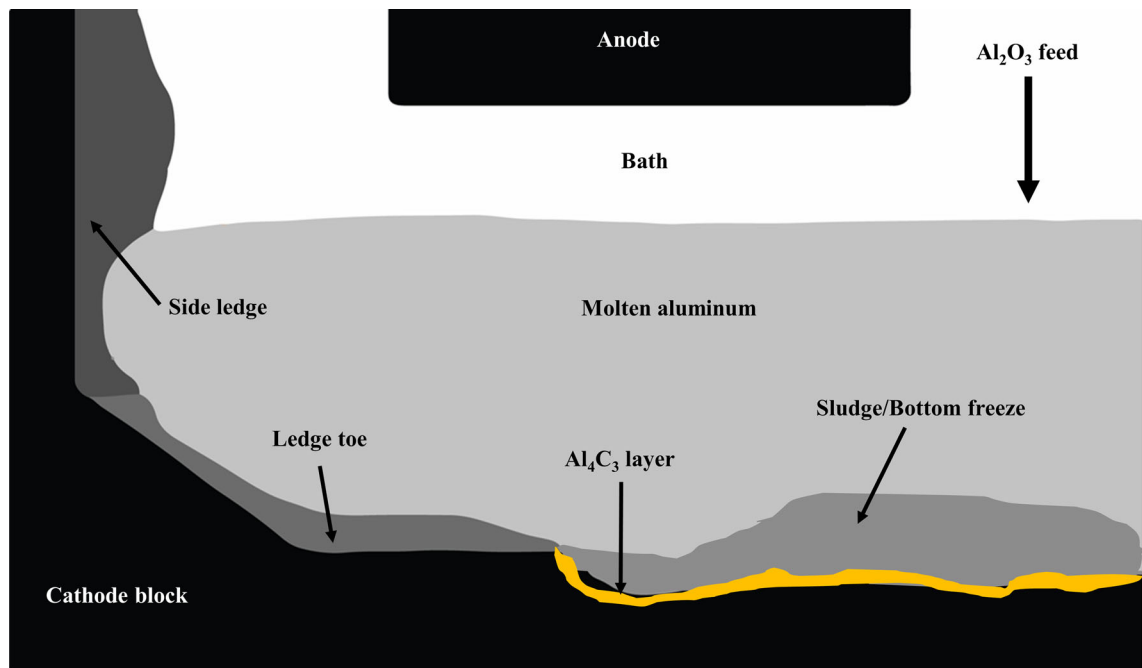


Fig. 1—Deposits at the carbon-metal interface of Hall-Héroult cells.

surface. In alumina point feeding cells, sludge mainly originates from alumina incomplete dissolution, collapse of top crust, anode change or failure in the heat balance of the cell.^[6] A typical sludge is a mixture of undissolved solid alumina particles and saturated bath with density around 2400 kg/m^3 , 20–50 pct alumina, 2–10 pct AlF_3 , and 2–5 pct CaF_2 .^[3,7] Bottom crust is caused by the complete solidification of sludge when its temperature reaches below the eutectic point of the sludge.^[8] According to Fallah Fini, *et al.*^[9] the most important factors that influence the sludge formation or dissolution are cell's hydrodynamics, operational temperature, electrolyte chemistry, physicochemical properties of alumina and alumina feeding techniques. It has to be underlined that sludge formation and solidification can be effectively reduced by keeping an appropriate superheat in the bath with respect to the acidity and alumina concentration in the cell.

C. Sludge Back Feeding Mechanisms

Once sludge is formed at the cathode surface, several mechanisms are stipulated to contribute to its back feeding into the bulk. The presence of a bath film between the carbon block and the metal was said to be related to sludge formation and dissolution.^[10] It was argued that sludge may be back fed through such a film wherein fluid flow is induced by interfacial tensions (IFT) differences.^[6,11] The bath film may also dissolve aluminum carbides formed at the carbon-aluminum interface, leading to net carbon losses of the block and cathode bottom wear.^[12–14] A layer containing such aluminum carbides at the cathode block-aluminum interface was observed in both industrial and laboratory

cells.^[15,16] However, hardly any laboratory study has explicitly shown signs of erosion visibly related to aluminum carbide formation and dissolution. Sludge may also be back fed into the bulk by the means of hydrodynamics. Accordingly, sludge could be dragged along the cathode surface by saltation caused by the moving metal and eventually be transported through the metal and dissolve in the bulk.^[17]

D. Cathode Grades in Modern Hall-Héroult Cells

The cathode material is of great importance, as it has to endure several electrical, thermal, and chemical phenomena during the lifetime of the cell. The optimal criteria for cathode lining material are as follows: chemical inertness, low permeability towards the environment, sufficient thermal and mechanical strength, ability to distribute current evenly, allow low CVD, controlled heat losses, and lowest possible cost.^[3] Carbon in the allotropic form of graphite is the material that fulfills the most of the latter requirements. With desired increased productivity, graphitized types of cathode blocks are attractive because of their higher thermal conductivity and lower electrical resistivity.^[18,19] However, graphitized cathode blocks in modern cells show higher wear rates because of increased amperage which has recently been correlated with high local current density and wear areas.^[20–22] Cells with graphitized cathode blocks of high thermal conductivity are more prone to bottom freeze, which increases the CVD.^[23] The thermal conductivity of the cathode block is also of major importance regarding the heat balance and the control of the thickness of the ledge and sludge formation. Controlled heat losses may also help to keep appropriate superheat, which disfavors sludge formation.

The impact of the cathode grade on sludge formation has not explicitly been investigated in literature. In fact, the industry has reported that distinctive cathode grades have shown variable propensities to form sludge. This experimental study will help to better understand the sludge formation phenomenon and to make further links between the graphitized cathode grade and the formation of deposits at the carbon-aluminum interface.

II. METHODOLOGY

A. Experimental Setup

Laboratory aluminum electrolysis tests were conducted using five industrial cathode grades (A, B, C, D, and E) provided by a Hall–Héroult cathode producer. The grades A to D are graphitized and the grade E is impregnated graphite (*i.e.*, graphitized then impregnated with pitch and rebaked). The properties of these grades were provided by the supplier and are listed in Table I.

From experience with these types of blocks, the industry has noticed that the sludge formation tendency differed typically from one grade to another. The sludge formation tendency of cathode grades, that was observed and reported by the industry, is $D = E > A > B > C$; D and E being the grades that forms the most sludge. This study aims to evaluate the behavior of the different grades of block in the experimental cells for comparison with the real-life behavior reported.

Rectangular experimental blocks of the five grades have been machined for laboratory electrolysis tests. All dimensions of the cell components are shown in Figure 2.

Alumina plates of 5 mm thickness are positioned on each cathode sidewall so that the current passes through the bottom. A plate of approximately 500 g of aluminum is placed at the bottom of the cell. The cell is then filled with 1700 g of industrial bath initially containing 10 pct (w/w) alumina with a cryolite ratio (CR) of 2.2. The anode is centered as the cryolite is being compacted in the cell. The cell is positioned inside a crucible made of Inconel placed inside a furnace. The temperature is measured in three locations: inside the bath, in the carbon sidewall, and inside the crucible. The type K thermocouples are placed inside alumina sleeves in order to protect them from bath corrosion and to prevent short-circuiting the system. The bath thermocouple is left inside the bath until the electrolysis is stopped.

The electrolysis tests are done at a 0.9 A/cm^2 current density for 8 hours under a N_2 atmosphere with a 2-cm ACD. The current is set to 73 A and is kept constant. The temperature and voltage are measured continuously during electrolysis. The bath is preheated between 1233 K and 1273 K (960 °C and 1000 °C) then the temperature is stabilized at 1233 K (960 °C) before the start of electrolysis. In order to highlight the impact of the cathode grade, no point feeding is used and all parameters are kept constant during the cell operation for all cathode grades. At the end of the electrolysis time, the electricity is cut off and the furnace is set to room temperature for cooling under nitrogen atmosphere. The time for the cell to reach room temperature is close to 30 hours in every case.

B. Autopsies

During its characterization, the cell is stored under argon atmosphere to avoid any oxidation reaction. In order to observe the deposits at the carbon-aluminum interface, the cell is cut using a diamond blade saw, as illustrated in Figure 3.

The cathode surface is separated by first cutting through the metal pad. The top of the cell is cut in two in the middle of the anode and the cell bottom part is cut in three positions as shown in Figure 3 (section a). After microscopic observations of the obtained slices of the cathode floor, cubes of the carbon-aluminum interface are carved with a diamond blade as shown in Figure 3 (section b).

C. Optical Microscopy

Microscopic observations of the carbon-aluminum interface are done with a stereomicroscope Leica MZ FLIII. Panoramic views of the interface are made in order to obtain size and position of deposits. The microscopic observation of the carbon-aluminum interface allows to measure the size of sludge, the extent of the ledge toe and the existence of erosion marks, if any.

D. X-Ray Diffraction (XRD) and Quantification of Chemical Composition

For the top part of the cathode block, samples are harvested from various regions of the bulk for chemical composition quantification. All deposits found at the bottom part of the block are harvested for

Table I. Cathode Block Properties at Room Temperature (*: Horizontal; **: Vertical)

Properties	A	B	C	D	E
Thermal Conductivity (W/m K)	125*	130*	145*	130*	130*
	112**	115**	135**	105**	105**
Electrical Resistivity ($\mu\Omega \text{ m}$)	12.0	10.5*	8.0*	10.5*	10.5*
		11.5**	9.0**	13.0**	13.0**
Open Porosity (pct)	18	14	15	20	14
Air Permeability (nPerm)	8	7	3	6	5

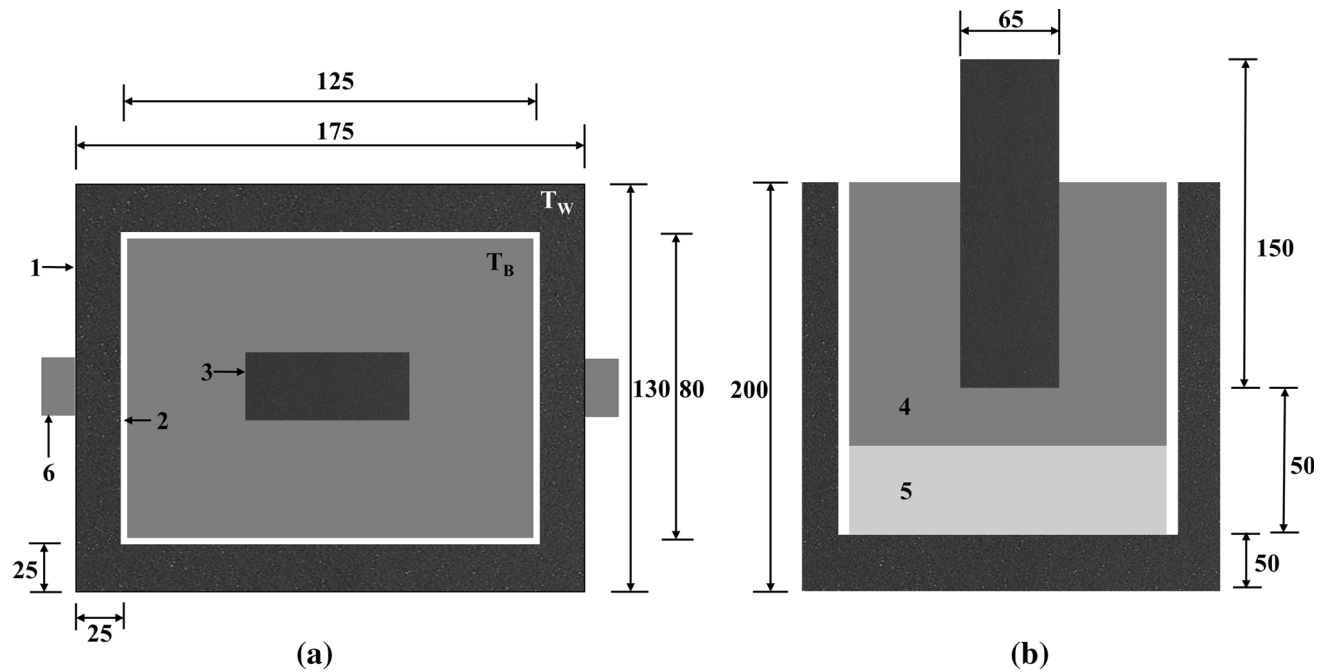


Fig. 2—Sizing of experimental Hall-Héroult cells for this study, top view (a) and side view (b). All dimensions are in millimeters (mm). 1: carbon crucible, 2: alumina plates, 3: anode, 4: bath, 5: aluminum, 6: bus bar. T_W and T_B refer, respectively, to the positions of the thermocouples in the sidewall and in the bath.

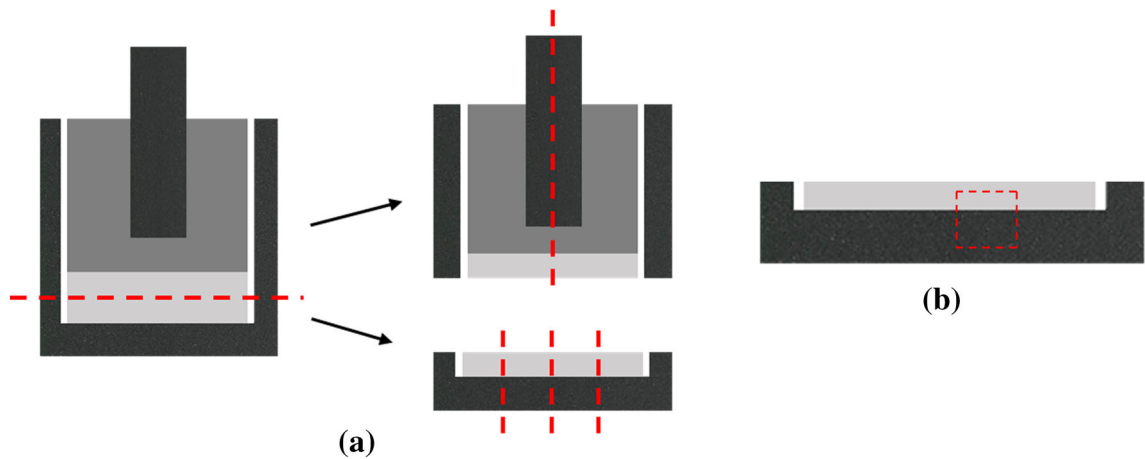


Fig. 3—Positions of cuts for deposit observation (red dashed lines); (a) cuts of the cell and cathode surface for microscopic sludge observations; (b) cutting for SEM observations of the carbon-aluminum interface.

quantification (sludge, ledge toe). The harvested samples are powdered using a ball mill, back loaded as pressed powder in a cavity and analyzed by XRD. The equipment used for XRD is a PANalytical X'Pert PRO MPD diffractometer and a PIXcel^{1D} detector with a nickel filter. An XRF Potflux Channel was used to determine the total calcium content of samples. The quantitative analysis of each sample is obtained by the Rietveld refinement.^[24] The CR based on stoichiometry (moles of NaF/moles of AlF_3) calculation is similar to the one used in previous studies on sludge formation as described by Allard, *et al.*^[2]

E. Scanning-Electron Microscopy (SEM)

The surface analysis for elemental cartography is done using the scanning electron microscope Hitachi S-4700 on samples of the carbon floor. The acceleration voltage is set to 20 kV. The intensity of the beam is 10 μA and the working distance 12 mm. The elemental analysis is done with an Oxford X-Mas 50 mm² energy-dispersive X-ray spectroscopy module (EDS). Electronic microscopy of the carbon-aluminum interface allows evaluating the topography of the interface and measuring the aluminum carbide layer typically formed under the metal.

III. RESULTS

For each experiment, the temperature was recorded with thermocouples in the bath, in the carbon sidewall and inside the Inconel crucible. Figure 4 depicts the temperature profile in the bath for the first five runs done for each cathode grade. The temperature of the bath is raised between 1233 K and 1273 K (960 °C and 1000 °C) before the start of electrolysis in order to assure that the bath is completely molten. Afterwards, the temperature of the bath is brought down to 1233 K (960 °C) before electrolysis is initiated. Immediately after the start of the electrolysis, there is a sudden increase in bath temperature due to the Joule effect. After about a thirty-minute period, the bath temperature suddenly drops by approximately 6 to 8 degrees in a one-minute timeframe, as it is observed in Figure 4. Subsequently, the bath temperature stabilizes back to 1233 K (960 °C) before it steadily decreases afterwards.

The heat generated by the Joule effect in the cell is transferred to the carbon walls of the experimental cell. Due to the constant nitrogen flow inside the crucible, the heat generated in the cell is lost to the surroundings by different heat transfer mechanisms, including conduction through the walls, convection at the surface of the bath and evaporation of the bath. On the other hand, there is considerable amount of radiative heat transfer between different elements, like the Inconel wall and the exterior of the cell. Consequently, the temperature of the bath is affected by a combination of the aforementioned heat transfer mechanisms. Nevertheless, the temperature recorded in the sidewall and in the crucible remained close to 1233 K (960 °C). Because of heat losses to the surrounding of the cathode block, the bath temperature has a tendency to decrease during operation. In order to keep the bath temperature as close as possible to 1233 K

(960 °C), the temperature of the furnace is adjusted accordingly (in the range between 1223 K and 1228 K), causing the small bumps on the bath temperature profiles in Figure 4. As it can be seen, all five grades have a similar bath temperature profile during electrolysis with a roughly 5 degree margin. At the end of the 8-hour electrolysis period, the furnace is turned off and the cell is let to cool down under nitrogen atmosphere.

After electrolysis, the bottom part of the block is cut in four sections as described in Figure 3. Each cut may or may not show a vivid sludge formation at the carbon-aluminum interface. Accordingly, the states of the carbon-aluminum interface associated with the temperature profiles of Figure 4 are presented in Figure 5.

As it is shown in Figure 5, the sludge profile is variable among the grades. An interesting cone-shaped sludge deposit was found near the center of the cell. Moreover, a variable amount of bath fills the peripheral corners of the cell bottom, which represents the ledge toe in this experimental study. The ledge toe becomes more and more thin as it elongates towards the center of the cathode floor, leaving a bath layer between the carbon and the metal. However, during autopsies, it could be seen that this layer is not always covering the total surface of the cathode. The thin bath layer observable at the carbon-aluminum interface of grades B and C has a yellowish color and bright yellow marks appear clearly in the carbon of grade C. The thickness of the ledge toe is often variable within a single cell, making the carbon-metal interface profile asymmetrical. In Figure 5 (section c), there is an apparent empty space in the metal which can be explained by the contraction of the metal during cooling. For each run illustrated in Figure 5, the characterization of the visible central sludge deposit and the ledge toe is summarized in Table II.

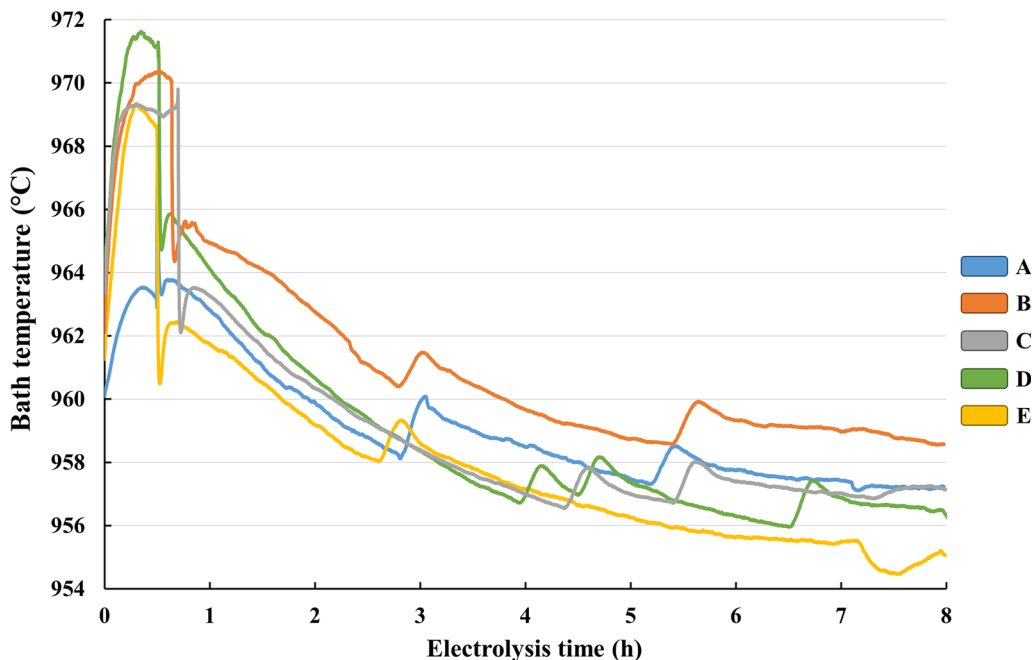


Fig. 4—Temperature profile of the bath for the five experimental grades during electrolysis.

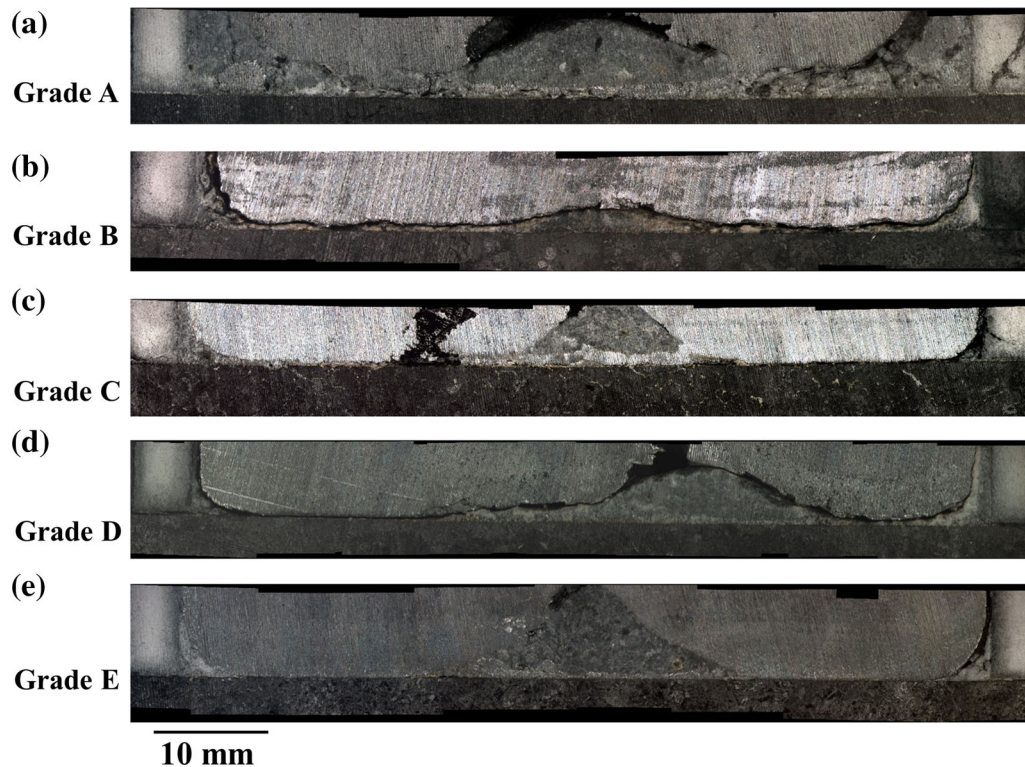


Fig. 5—Microscopic observations of the carbon-aluminum interface profile in the center of the cell for the five cathode grades; grade A (a), grade B (b), grade C (c), grade D (d), and grade E (e).

For the five runs shown in Figure 5/Table II, the bulk of the electrolyte has an alumina content between 4 and 11 with a CR lower than 2 at the end of the electrolysis. The composition of the ledge toe has a higher alumina mass percentage and CR than the initial bath. Accordingly, it is a mixture of undissolved alumina and saturated bath. The central sludge deposits are also alumina-saturated bath and undissolved alumina with a CR less acidic than the initial composition of the bath (CR of 2.2 and 10 pct alumina), which is also saturated bath. Besides, the sludge composition shown in Table II shows little variability; nevertheless, the sludge profiles from Figure 5 differ significantly. However, when comparing each run with close conditions, it is evident that the size, shape, location, and composition of the sludge vary considerably from one run to the other (Figure 6).

Nonetheless, in every case, the average CR of the ledge toe in impregnated graphite (grade E) is the lowest among all the grades. Moreover, grades B and C, which have high thermal/electrical conductivities, have the highest average CR while grade E has the lowest value. As sections c and d in Figure 6 reveal, the number of times that samples of central sludge were analyzed reflects the actual number of times that central sludge had formed. Evidently, grade A is the grade that contained the most sludge in this study although it was listed as the grade with second highest sludge propensity by the industry. Moreover, a distinct central deposit was found only once for grade B.

A. Observations Related to the Post-Mortem Analysis of the Bulk Bath

The interior of the cell above the metal was also analyzed. It was found that the electrically insulating alumina plates were being dissolved during the experiments, implying an uncontrolled alumina feeding to the bath. The maximum point of erosion of the plates, shown on Figure 7, was at the bath-air interface, due to bubble-induced movement of the surface and the alumina dissolution in the low oxygen bath coming from the anode.

As it is shown in Figure 7, the darker electrolyte above the tip of the anode (*i.e.*, zone 1) is quite porous, caused by the bubbling at the anode. The electrolyte below the anode (*i.e.*, zone 2) is much more packed. The characterization of samples taken in the indicated zones reveals a gradient of alumina concentration, CR and density from the point of erosion to the cathode bottom. Samples from zone 2 have an average alumina concentration and acidity similar to zone 1. However, samples collected in zone 3 (gray bath between the metal and the alumina plate) have a higher average alumina content and CR, which is similar to the bottom deposits. Zone 3 is the farthest region from the anode tip, which is a highly agitated area; therefore, it may be the ideal location of alumina accumulation when it precipitates. The alumina concentration exceeds saturation in zone 3, in the central sludge and in the ledge toe. Other laboratory scale electrolysis experiments have shown

Table II. Total Alumina Content (from Rietveld Refinement) and Cryolite Ratio of Central and Ledge Toe Sampled in Cells from Fig. 5

Cathode Grade	Central Sludge		Ledge Toe	
	CR	Al ₂ O ₃ (wt pct)	CR	Al ₂ O ₃ (wt pct)
A (Graphitized)	2.8	22	2.2	23
B (Graphitized)	N/A	N/A	2.6	18
C (Graphitized)	2.9	28	2.6	24
D (Graphitized)	2.6	20	2.8	20
E (Graphitized)	2.9	19	2.1	19

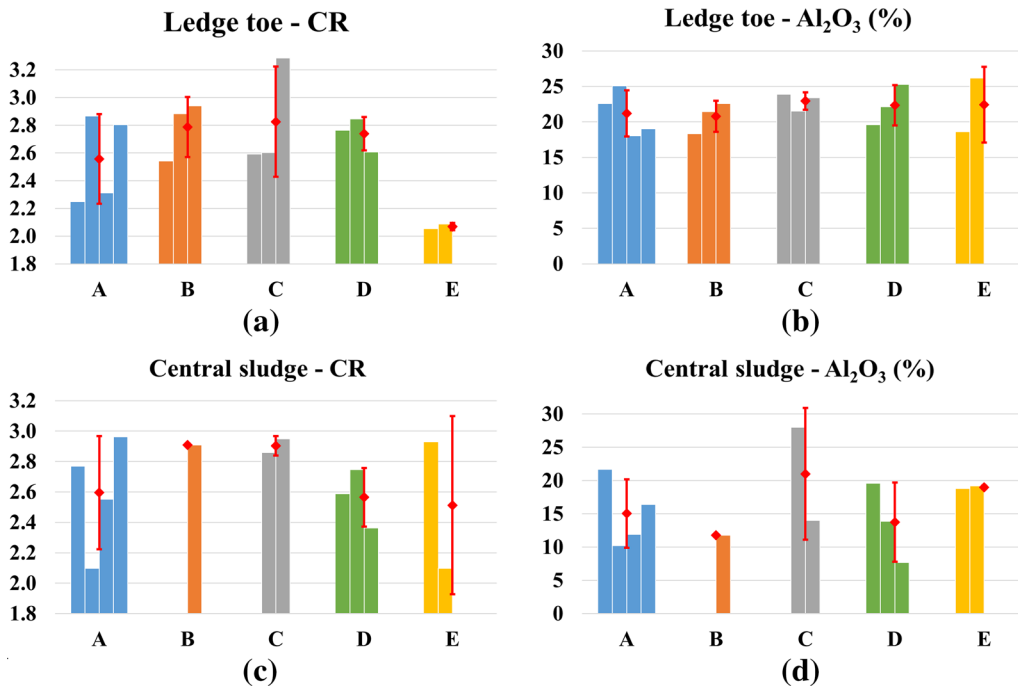


Fig. 6—Characterization summary of all experiments; the red markers are the average values by grade with the standard deviation; CR of ledge toe (a), total alumina mass percentage of ledge toe (b), CR of central sludge (c), and total alumina mass percentage of central sludge (d).

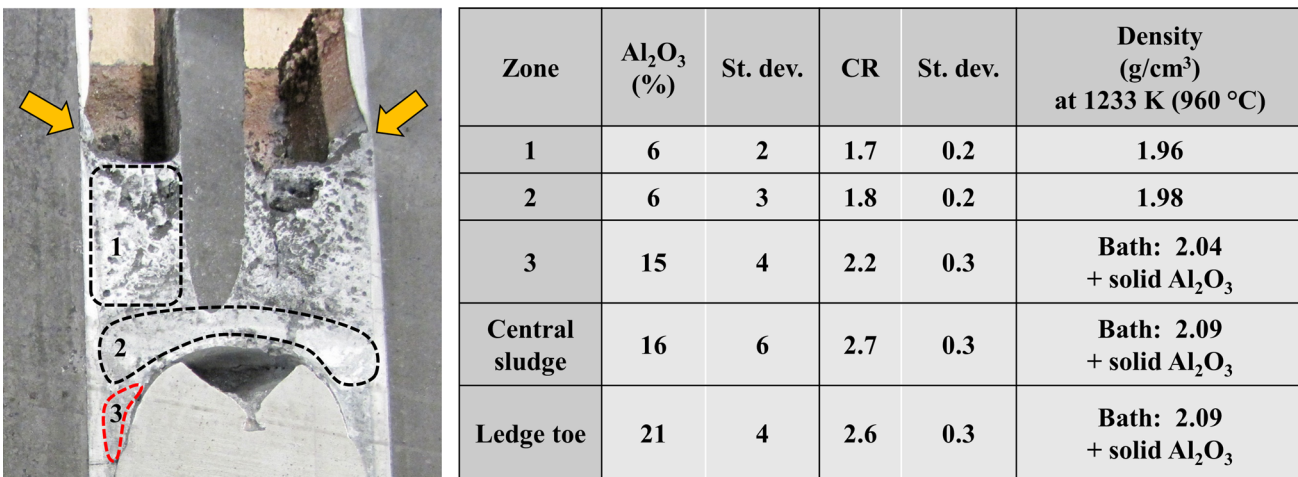


Fig. 7—Transversal cut of a typical experimental cell and the average alumina mass percentage and CR of the indicated zones; the yellow arrows indicate the typical region where the maximum erosion of alumina plates occurs. The region circled in red indicates that it is supersaturated in alumina.

the presence of sludge containing 25 pct alumina and a CR of 2.2 (*i.e.*, acidic).^[25] However, those experiments were done with alumina point feeding while the runs presented in this paper had no alumina point feeding. In this experimental study, the initial state of the electrolyte is a mixture of liquid bath and solid undissolved alumina. Considering the additional alumina is coming from the alumina plate erosion, it is not surprising to find considerable amounts of sludge at the bottom of each cell. This increasing of alumina concentration to the system originates from the corrosion of the alumina plates caused by the low oxygen content of the bath surrounding the anode region. The XRD analysis of the samples shown in Figure 7 reveals that the composition of the electrolyte at the end of the run, above the metal, has on average 6 pct Al_2O_3 with an average CR of 1.8. According to the phase diagram of the experimental system Al_2O_3 - AlF_3 - NaF - CaF_2 , the onset of the experiment is within a two-phase region, requiring alumina precipitation enrichment of the bottom of the cell.

According to Figure 8, the acidification of the bulk has a stronger effect on the cryolite liquidus than on the alumina liquidus. Samples above the metal reached the liquid zone while deposits under the metal stayed in the alumina and bath mixture phase. The alumina concentration in the bulk at the end of the experiments suggests that the bath (initially supersaturated) reaches the saturation line during electrolysis. Upon alumina consumption from electrolysis, the alumina concentration in the bulk decreases. The bath depleted from alumina after electrolysis is circulated towards the top of the cell by the means of the bubble agitation, leading to more

alumina from the plates getting dissolved, as observable in Figure 7. The undissolved alumina from the initial bath or the corrosion of the plates precipitates to the bottom.

B. Observations on the Profile Characteristics of the Bottom Deposits

Although sludge profiles vary from one experiment to the other, some distinctive characteristics of each cathode grade with regard to sludge and other bottom deposits have been noted and summarized in Table III.

C. Observations on the Behavior of Voltage During the Electrolysis

The voltage for each run is measured continuously and the amperage is kept constant at 73 A. When current is launched, the voltage starts around 5.0 V, then decreases between 4.6 and 4.9 V before it generally starts to rise. The tendency for highly electrically conductive grade C and impregnated graphite grade E is to start rising after roughly 3 hours of electrolysis. For grade B, the voltage typically starts to rise after 4 hours of electrolysis while graphitized grades A and D present steadier voltage behaviors under 5 V during the 8-hour operation period. The average voltage for each grade is presented in Figure 9.

It does not seem likely that the voltage behavior in this study is directly correlated with the amount of sludge at the carbon-aluminum interface. On the other hand, as mentioned in Table III, the cathode grade C

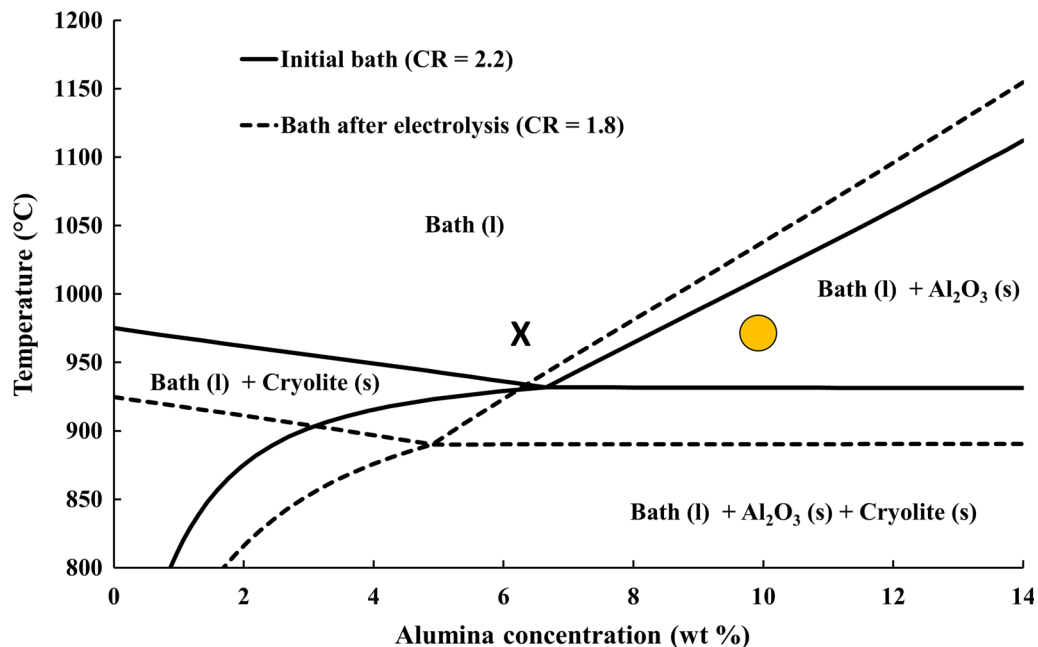


Fig. 8—Thermodynamic phase diagram from FactSage of the system Al_2O_3 - AlF_3 - NaF - CaF_2 ; the yellow circle (yellow filled circle) and X mark indicate respectively the initial condition of electrolysis and the composition of the bulk bath at the end of the run.

Table III. Qualitative Observations of Carbon-Aluminum Interface for Each Cathode Grade

Cathode Grade	Observations
A (Graphitized)	<ul style="list-style-type: none"> - High amount of ledge toe that stretches towards a continuous thick layer (> 1 mm) - The thick layer always covers the entire area of the carbon-aluminum interface
B (Graphitized)	<ul style="list-style-type: none"> - The ledge toe is evenly distributed around the perimeter of the cell - The ledge toe is not evenly distributed, it tends to be thicker in some areas, leaving other regions free of deposits or covered with a thin layer (< 1 mm)
C (Graphitized)	<ul style="list-style-type: none"> - Just like grade B, the ledge toe is not evenly distributed, but to a higher extent - The bath layer is thin (< 1 mm), non-continuous and with bright yellow marks - Erosion of the carbon surface is observed
D (Graphitized)	<ul style="list-style-type: none"> - High amount of ledge toe is observed, not evenly distributed along the perimeter - The thin layer (< 1 mm) does not cover the total area of the cathode surface - A small amount of central sludge is observed
E (Graphitized + Impregnated)	<ul style="list-style-type: none"> - An uneven ledge toe distribution is noticed - The thin layer (< 1 mm) does not cover the total area of the cathode surface - Variable amounts of central sludge are observed

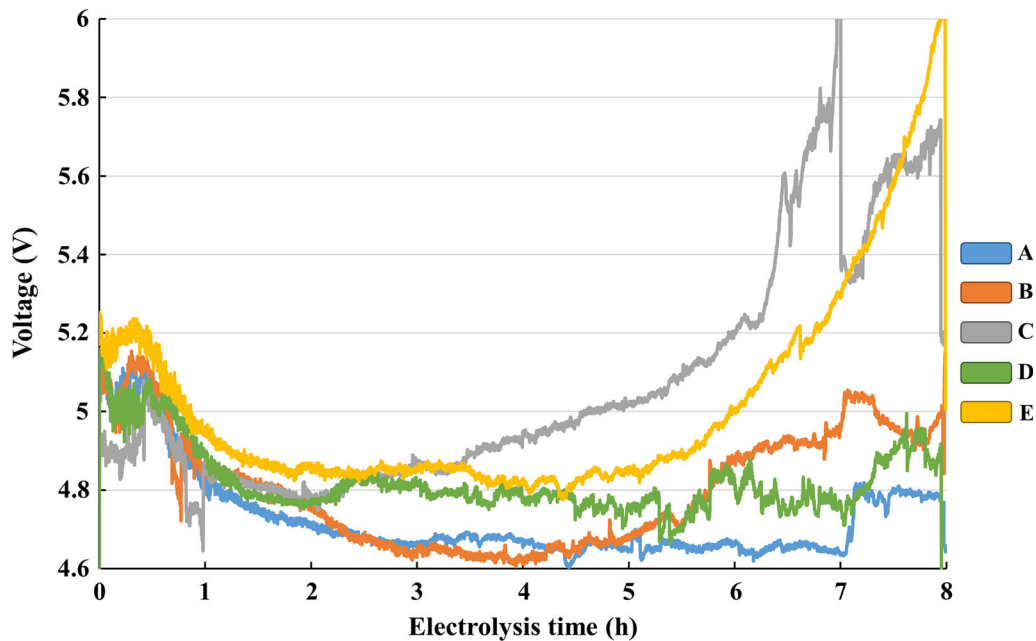


Fig. 9—Average voltage by cathode grade.

also stood out for its visible erosion marks, which may explain the voltage rise. On the contrary, no visible signs of erosion were observed on impregnated graphite grade E.

D. SEM-EDS Observations of the Carbon-Aluminum Interface

The highest erosion is located where the tip of the elongated ledge toe or thin layer disappeared. Moreover, SEM-EDS observations of the carbon-aluminum interface revealed the presence of a layer containing aluminum covering the carbon surface and going inside the wear pits (Figure 10).

The green layer containing aluminum in the SEM imaging appears to be aluminum carbide, which is nowadays thought to be highly responsible for cathode wear. This layer was observed with all five grades. The high wear, illustrated in Figure 10, suggests that the electrochemical formation of aluminum carbides and its subsequent dissolution in bath (from ledge toe or thin layer) is faster for cathode grades with a film that does not cover the entire cathode surface. Moreover, it may explain the voltage rise observable for grade C. The eroded parts of the carbon surface filled with bath may have prolonged the current paths around the pits, thus provoking voltage rise that is observed especially for grade C. The thickness of the aluminum carbide layer

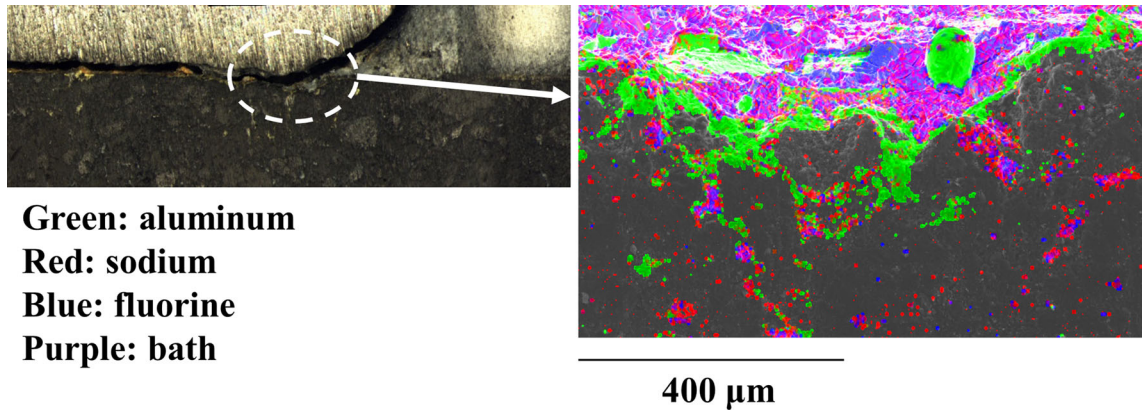


Fig. 10—SEM-EDS observation of the indicated zone of the carbon-aluminum interface for grade C.

was measured for each block and an apparent correlation with the open porosity of the cathode grade has been previously established.^[26] In Figure 10, the aluminum carbide layer appears to be following the morphology of the carbon surface. Accordingly, erosion is taking place when aluminum carbides form around a small piece of carbon before dissolving inside the bath infiltrated in the pores. The detachment of the surrounded carbon piece accounts for the growing pit.

IV. DISCUSSION

Sludge formation is influenced by a myriad of phenomena that interact with each other during the regular operation of a cell. The major factors are temperature of the bath, interfacial phenomena, hydrodynamics, bath chemistry, and alumina feeding strategy.^[9] Since no point feeding was used in this study, the impact of feeding strategy on sludge formation will not be discussed and reader is encouraged to refer to Fallah Fini *et al.*^[9] Since the cathode block is an obligatory passage for heat, mass and electricity, consequently the aforementioned factors (*i.e.*, temperature of the bath, interfacial phenomena, hydrodynamics, bath chemistry, and alumina feeding strategy) should also be influenced by the thermal, electrical, and structural properties of the cathode block.

A. Effect of Temperature

The proper dissolution of alumina and avoidance of sludge formation call for an appropriate superheat of the bath. Since close to half of the heat losses go through the carbon walls of the cathode,^[3] the heat balance of the cell is partially controlled by the thermal conductivity of the cathode block. Expectantly, the cathode grade should have an impact on sludge formation through the cell heat balance. As it is seen in Table I, the five cathode grades have different horizontal and vertical thermal conductivities, which suggests variable heat flows depending on the grade, thus variable sludge profiles. As mentioned earlier, the bath is heated by the Joule effect during electrolysis and cooled by several

heat transfer modes. The heat generated inside the cell is transferred by conduction through the graphitized cathode block. The heat lost through the furnace walls and the nitrogen gas flow account for the convective cooling on the exterior of the cathode block. Moreover, the cell is subject to radiative heating coming from the furnace. Due to the complex combination of heat transfer modes affecting the bath temperature, it is not obvious to clearly discern the impact of the thermal conductivity of the cathode block on the heat transferred by conduction through the carbon phase. Nevertheless, during the more stable period of electrolysis (after the sudden temperature increase and decrease seen in Figure 4), the experimental cooling rate of the bath was calculated for each run and is plotted in Figure 11.

Consequently, it was found that the grade with a significantly higher average thermal conductivity (*i.e.*, grade C) had the fastest cooling rate during the electrolysis. This foreseeable result highlights the sensitivity of cathode grades to heat losses even though those grades have close thermal conductivities. The different thermal behaviors seen with the experimental cells yet again emphasize the fact that the heat balance of the cell is greatly influenced by the cathodic carbon block. Knowing that heat losses must be well controlled in order to keep an appropriate superheat and limit sludge formation, the choice of cathode grade is important as it directly influences the rate and uniformity of heat losses. More uniform heat losses should help to control the position of the liquidus isotherm, thus keeping an appropriate uniform protective ledge. This may be easier to achieve by ensuring that the thermal conductivity of the carbon block is as uniform as possible in the whole block. However, it is known that the thermal conductivity of the cathode block changes during the life time of the cells and such changes are due to different phenomena that the cathode block endures.^[27] Therefore, there must be a correlation between the cathode block raw microstructure (*i.e.*, initial open porosity), infiltration depth of the bath and dynamic thermal conductivity during the operation. In fact, in a recent laboratory study, using similar cathode grades, the impregnated graphite with lower porosity had a lower bath penetration depth than non-impregnated

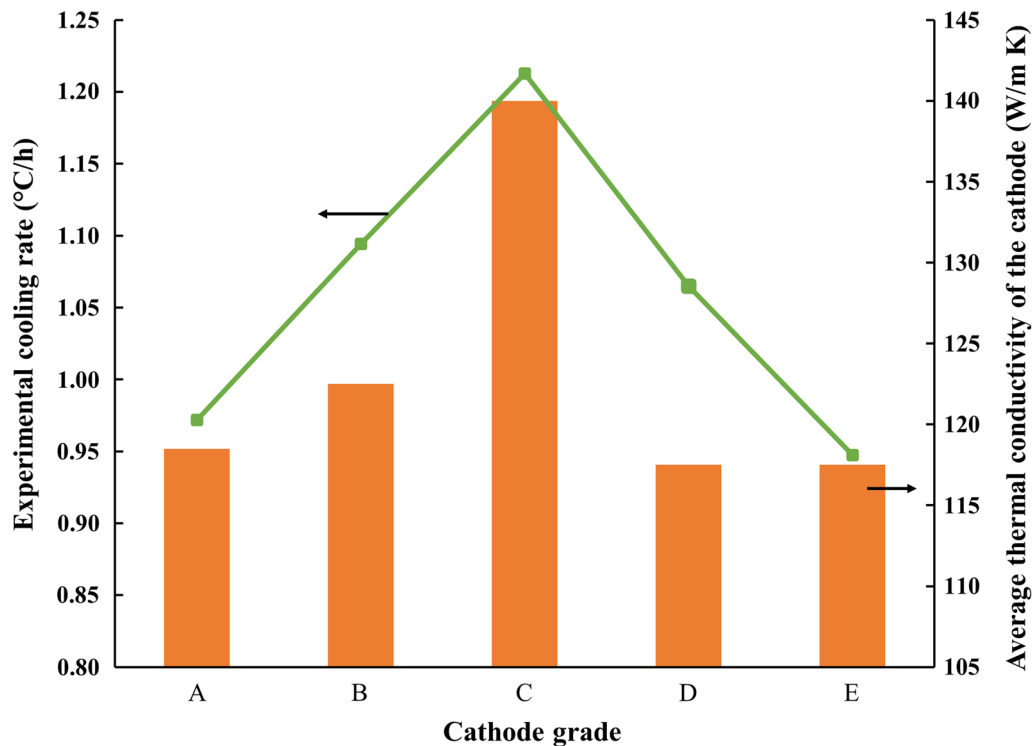


Fig. 11—Average cooling rate per cathode grade and average thermal conductivity of block: average conductivity was obtained by averaging the horizontal and vertical conductivities.

graphite.^[28] Consequently, in the current study, the impregnated grade E must have been filled with a smaller volume of bath. Despite its same raw thermal conductivity as grade E, grade D showed a significantly faster cooling rate than E during electrolysis. This could be due to a more intense change of thermal conductivity for grade D, resulting from a large bath infiltration enhanced by the higher open porosity of grade D. Although pitch impregnation of graphite blocks is typically used to decrease porosity and increase wear resistance, the pitch impregnation of grade E, while differentiating it from grade D, may have also helped to reduce the rate of heat losses.

B. Effect of Interfacial Tension (IFT)

At first, the formation of sludge was foreseeable because the initial bath composition was in the two-phase region (Figure 8). When central sludge was found, it was connected to the ledge toe by a bath layer more or less thin, as pictured in Figure 5. A similar bath layer was observed in previous experiments and was speculated to be resulting from the ledge toe/sludge displacement by MHD on the cathode block surface.^[16] Moreover, the existence of a bath film between the carbon and the aluminum was evoked and said to be related to the formation and dissolution of sludge.^[10] Studies on IFT between cryolitic melts and aluminum showed that the IFT between the cryolitic melt and the molten aluminum increases with increasing AlF_3 because of the higher activity of sodium.^[6,29,30]

Accordingly, it was suggested that a movement in the liquid bath film can be induced if there is an IFT gradient between the bath at the aluminum-electrolyte interface and the film at the carbon-aluminum interface. Moreover, the direction of the movement of the film is from the region of lower IFT (*i.e.*, low AlF_3) to the region of higher IFT (*i.e.*, high AlF_3). The so-called Marangoni flow can back feed the sludge into the bulk if the direction is from the carbon-aluminum interface to the bulk. As it was mentioned previously, the thickness of the bath layer was variable among grades in this study. For grade A, the bath layer was thicker and clearly distinguishable. In order to further discuss the influence of IFT and cathode grade, a schematic diagram is proposed in Figure 12.

The bath layer found below the aluminum seen in Figure 12 (section a) has a lower CR than the central sludge yet a similar alumina concentration. Also, a thin vertical bath film separating the aluminum pad and the alumina plate connects the bath layer and the bulk. Moreover, there is a gradient of CR from the bulk to the sludge, thus an IFT gradient. This suggests that central sludge may be back fed into the bulk through the bottom layer and the thin vertical film. As a result, alumina may back feed if fresh bath from the bulk can be circulated to the sludge through this film. Besides, the ability of the cathode block to pass sodium may tamper with the sodium depletion of the vertical bath film. As it is depicted in Figure 12 (section b), a high sodium diffusion through the cathode block and alumina plate may shift the CR of the bath film to more acidic, thus

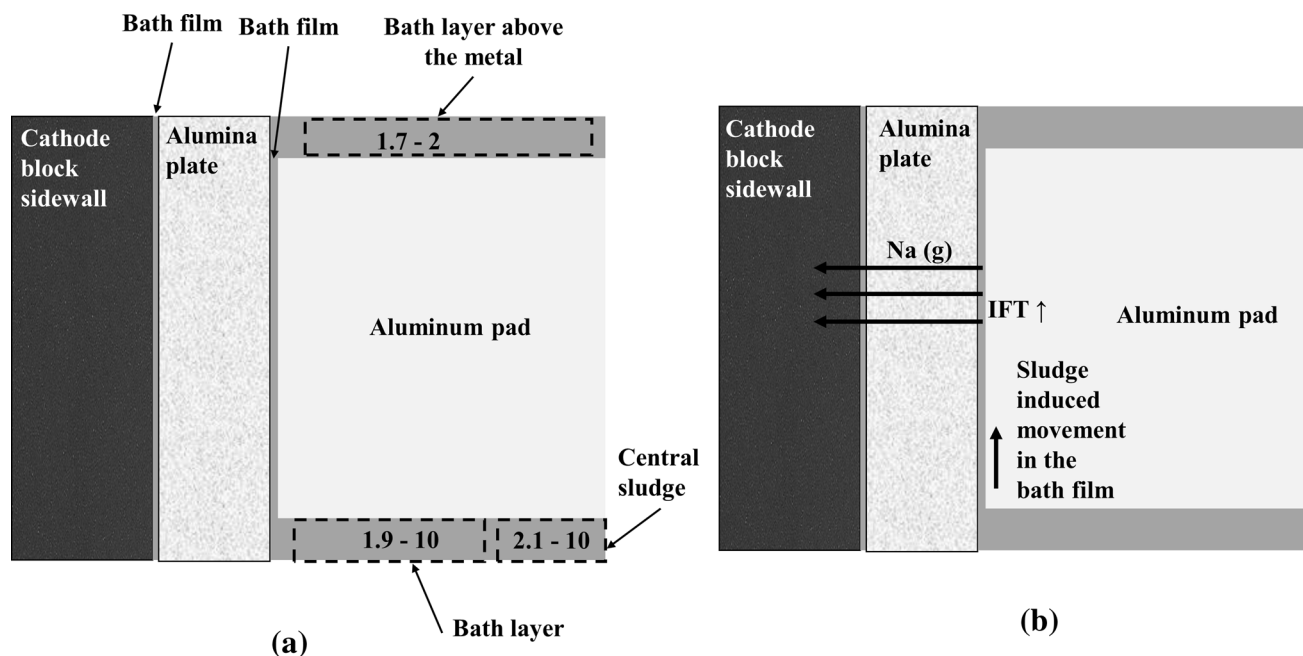


Fig. 12—(a) Bath film connecting the bottom bath layer and the bulk (CR—alumina pct) for one run with cathode grade A, (b) film movement induced by sodium losses in cathode block.

promoting sludge back feeding through this vertical film. The effective diffusion of sodium gas through the carbon may depend on its porosity, tortuosity and air permeability.^[31] Therefore, cathode grades with high sodium diffusivity may tend to have a lower CR in the bath between the sidewall and the metal, thus drawing mass transfer towards the bulk and promoting sludge back feeding. In this study, grade A was the grade with the highest air permeability, which may further explain the thicker bath layer observed. Other than the fact that grade A had a thick bath layer, no correlation was found between the cathode properties and the acidity of the bath in the bulk or in any other deposit. Nevertheless, if the cathode block has the potential to alter the acidity of the bath, it may well lead to IFT gradients between the bottom deposits and the bulk, thus inducing Marangoni flows that affect sludge accumulation or back feeding. Furthermore, the Rietveld refinement of the bath samples at the aluminum-bath interface has shown too much variability to prove the presence of a consistent layer of bath rich in alumina that could sink through the metal pad. The agitation in the bath from the anode gas release, seen in Figure 7, may have caused such variability of concentration in the bath above the metal. With considerable agitation due to bubble movement and the small size of the cell, it is perceivable that hydrodynamics also play a major role in formation or dissolution of sludge.

C. Effect of Hydrodynamics

Irrespective to IFT induced movement, bubble movement and magneto-hydrodynamics are the most effective forces in the cell. In industrial cells, proper bubble agitation contributes to dissolution of fed alumina

particles while oscillation of the bath-metal interface leads to losses in current efficiency.^[32] Also, the large molten metal pad is constantly in movement due to MHD forces. In this study, it would take a considerable movement of the metal pad in order to lift the bottom sludge deposits right up into the bulk. With regard to this fact, Kalgraf and Torklep^[17] have argued that the sludge back feeding process may be governed by the laws of sediment transport. Considering the fact that the sludge is a mixture of crystallized alumina particles and a saturated bath, sufficient turbulence of the metal pad movement could allow the sludge to be lifted (*i.e.*, back-fed) into the bulk through the metal pad. In the present study, there is no obvious reason to believe that there was a sufficient metal pad movement from MHD near the cathode surface to transport sludge in such a manner. The agitation inside the cell is more likely to originate from bubble movement at the anode. Signs of agitation in the metal pad were only observed during the autopsy of a cell cooled during electrolysis. However, agitation signs were only observed in the ACD, which may be attributed to bubble-induced movement or aluminum forming during cooling. Nevertheless, it is not clear at this point how the cathode grade can impact the sludge dissolution process through sediment transport-like movement.

V. CONCLUSIONS

Laboratory electrolysis tests with five different graphitized cathode grades were performed to study the formation of sludge at the cathode surface. This study has revealed the formation of a distinct conical sludge deposit near the center of the carbon-aluminum

interface for each grade, despite the absence of point feeding during electrolysis. The central sludge and ledge toe deposits had an alumina mass percentage ranging from 10 to 25 pct and a CR from 2.4 to 2.9. No correlation was found between the composition of the bottom deposits and the cathode grade in this study.

The profile of sludge was variable among cathode grades, which further suggests that the cathode grade has an impact on sludge formation. However, no clear correlation between the thermal conductivity of the cathode block and the temperature profiles was found, due to the complex array of heat transfers involved during the experiments. The observable temperature profile variations testify of the sensibility of the experimental setup used in this study. Nevertheless, a certain amount of sludge was always found at the carbon-metal interface in each experiment. The phenomenon of sludge formation may be repeatable, granted that conditions inside the cells (especially temperature profiles) are replicated.

The higher CR of the central sludge vs the CR of the bulk suggested an induced movement in the vertical bath film, resulting from IFT difference between the bulk and the bottom of the cell, while enhancing the back feeding of the sludge. Therefore, the propensity of a cathode block to alter the acidity of the vertical bath film between the metal and the sidewall may then contribute to induce sludge back feeding. Cathode grades with high permeability may be more prone to sludge back feeding by IFT-driven movement.

The wear of the carbon-aluminum interface may be faster for the cathode grades with a film that partially covers the cathode surface. A layer of aluminum carbide is observed with SEM-EDS inside the erosion pits. The erosion pits in the cathode surface may contribute to the voltage rise. In order to alleviate the problem of pit formation (*i.e.*, erosion of cathode surface), other methods such as copper inserts can be used to lower the CVD, reduce the MHD forces and make current paths more uniform. The use of such inserts in combination with graphitic cathode grade was recently predicted to have an increased interest in a near future.^[23] Furthermore, the use of such cathode grades with lower electrical and thermal conductivities may help to keep a better control over the heat balance, hence reduce sludge formation and its detrimental drawbacks.

REFERENCES

1. X. Liao and H.A. Oye: *Light Met. 1999, Proceedings of the International Symposium*, 1999, pp. 621–27.
2. F. Allard, G. Soucy, and L. Rivoaland: *Metall. Mater. Trans. B*, 2014, vol. 45B, pp. 2475–85.
3. K. Grjotheim, and H. Kvande, eds., *Introduction to Aluminium Electrolysis - Understanding the Hall-Heroult Process*, 2nd ed., Aluminium-Verlag, Düsseldorf, Germany, 1993.
4. Y. Song, J. Peng, Y. Di, Y. Wang, and N. Feng: *Can. Metall. Q.*, 2017, vol. 57. Ahead of Print.
5. M. Sorlie and H.A. Oye: *Cathodes in Aluminium Electrolysis*, 3rd ed., Aluminium-Verlag, Düsseldorf, 2010.
6. T. Utigard and J. M. Toguri: *Light Met. 1991, Proceedings of the International Symposium*, 1991, pp. 273–81.
7. F. Allard, G. Soucy, L. Rivoaland, and M. Désilets: *J. Thermal Anal. Calorim*, 2014, vol. 119, pp. 1303–14.
8. P.Y. Geay, B.J. Welch, and P. Homs: *Light Met. 2001, Proceedings of the International Symposium*, 2001, pp. 541–47.
9. M. Fallah Fini, G. Soucy, M. Désilets, P. Pelletier, D. Lombard, and L. Rivoaland: *Alumina, Aluminum, Proceedings of the International Symposium on ICSOBA*, 2017, vol. 42, pp. 987–96.
10. T. Li, S. T. Johansen, and A. Solheim: *TMS Light Met.*, 2015, pp. 831–36.
11. T. Utigard: *Light Met. 1999, Proceedings of the International Symposium*, 1999, pp. 319–26.
12. X. Liao and H.A. Oye: *Light Met. 1998, Proceedings of the International Symposium*, 1998, pp. 667–74.
13. B. Novak, K. Tschöpe, A.P. Ratvik, and T. Grande: *Light Met. 2012, Proceedings of the International Symposium*, 2012, pp. 1343–48.
14. A. Zoukel, P. Chartrand, and G. Soucy: *Light Met. 2009, Proceedings of the International Symposium*, 2009, pp. 1123–28.
15. B. Novak, A.P. Ratvik, Z. Wang, and T. Grande: *Light Met. 2018, Proceedings of the International Symposium*, 2018, pp. 1215–22.
16. M.A. Coulombe, G. Soucy, L. Rivoaland, and L. Davis: *Metall. Mater. Trans. B*, 2016, vol. 47B, pp. 1280–95.
17. K. Kalgraf and K. Torklep: *Light Met. 1998, Proceedings of the International Symposium*, 1998, pp. 455–64.
18. Z. Wang, S. Nobakhtghalati, A. Store, A. Solheim, K. Tschöpe, A.P. Ratvik, and T. Grande: *Light Met. 2016, Proceedings of the International Symposium*, 2016, pp. 895–902.
19. K. Tschöpe, A. Store, S. Rorvik, A. Solheim, E. Skybakmoen, T. Grande, and A.P. Ratvik: *Light Met. 2012, Proceedings of the International Symposium*, 2012, pp. 1349–54.
20. K. Tschöpe, A. Store, E. Skybakmoen, A. Solheim, T. Grande, and A.P. Ratvik: *Light Met. 2013, Proceedings of the International Symposium*, 2013, pp. 1251–56.
21. E. Skybakmoen, S. Roervik, A. Solheim, K.R. Holm, P. Tiefenbach, and O. Ostrem: *Light Met. 2011, Proceedings of the International Symposium*, 2011, pp. 1059–66.
22. J.-M. Dreyfus and L. Joncourt, in *Light Metals 1999*, C.E. Eckert, ed., The Minerals, Metals and Materials Society (TMS), Warrendale, PA, 1999, pp. 199–206.
23. L. Rivoaland: *Bauxite, Alumina, Alum.*, *Proceedings of the International Symposium on ICSOBA*, 2016.
24. F.R. Feret: *Light Met. 2008, Proceedings of the International Symposium*, 2008, pp. 118–28.
25. F. Allard, M.A. Coulombe, G. Soucy, and L. Rivoaland: *Light Met. 2014, Proceedings of the International Symposium*, 2014, pp. 1233–38.
26. J.-R. Landry, M. Fallah Fini, G. Soucy, M. Désilets, P. Pelletier, L. Rivoaland, and D. Lombard: *Light Met. 2018, Proceedings of the International Symposium*, 2018, pp. 1229–33.
27. A. Yurkov: *Refractories for Aluminium Electrolysis and the Cast House*, 1st ed., Springer, Switzerland, 2015.
28. M. Brassard, M. Soucy, M. Désilets, and D. Lombard: *Can. Metall. Q.*, 2016, vol. 55, pp. 356–64.
29. M. Korenko: *J. Chem. Eng. Data*, 2008, vol. 53, pp. 794–97.
30. E.W. Dewing and P. Desclaux: *Metall. Mater. Trans. B*, 1977, vol. 4B, pp. 555–61.
31. Z. Wang, E. Skybakmoen, and T. Grande: *Light Met. 2009, Proceedings of the International Symposium*, 2009, pp. 353–58.
32. J. Thonstad, G. Felner, G.M. Haarberg, J. Hives, and H. Kvande: *Aluminium Electrolysis—Fundamentals of the Hall-Heroult Process*, 3rd ed., Aluminium-Verlag, Düsseldorf, 2001.